Journal of Controlled Release 396 (2026) 115068

Contents lists available at ScienceDirect

Journal of Controlled Release

journal homepage: www.elsevier.com/locate/jconrel

# Chemoimmunotherapeutic sealants for postsurgical adjuvant therapy of malignant tumors

Xueling Tang [a,1], Jianrong Wang [a,1], Lin Chen [a], Yan Zhao [a], Li Cao [b], Huanli Sun [a,*], Zhiyuan Zhong [a,b,*]

[a] State Key Laboratory of Bioinspired Interfacial Materials Science, and Biomedical Polymers Laboratory, College of Chemistry, Chemical Engineering and Materials Science, Soochow University, Suzhou 215123, PR China
[b] College of Pharmaceutical Sciences, Soochow University, Suzhou 215123, PR China

ARTICLE INFO

*Keywords:*
Post-surgery adjuvant therapy
Fibrin sealant
Immunosuppressive tumor microenvironment
Immunogenic cell death
cancer immunotherapy

ABSTRACT

Surgery followed by adjuvant therapy is a mainstream clinical strategy for advanced tumors. It is, however, often the case that tumors will recur due to incomplete depletion of residual cancer cells and surgery-triggered immunosuppressive milieu. Herein, we report a chemoimmunotherapeutic fibrin sealant (CI-sealant) as a new postsurgical adjuvant therapy that converts the surgical cavity into an in situ "drug-immune depot" with localized release of immunogenic docetaxel/volasertib dual-drug nanocombo (iNCombo) and galunisertib, a TGF-β inhibitor that relieves immune suppression. The iNCombo elicits strong apoptosis and immunogenic cell death (ICD) in diverse tumor cells, effectively stimulating dendritic cell maturation. CI-sealant induces ICD of residual cancer cells in situ, facilitates T-cell activation and infiltration, and increases the proportion of M1 macrophages, effectively reversing immunosuppression and boosting antitumor immunity in a postoperative 4T1 triple-negative breast cancer model. Post-surgery adjuvant therapy with CI-sealant significantly prevents tumor recurrence in both murine 4T1-Luc breast tumor and B16F10 melanoma models. This chemoimmunotherapeutic sealant opens a promising strategy for postsurgical adjuvant therapy of malignant tumors.

## 1. Introduction

Surgical resection is the cornerstone of solid tumor treatment in clinical practice [1,2]. Concomitantly, hemostatic and wound-healing strategies, such as fibrin sealants, are routinely applied, followed by adjuvant therapy (e.g., chemotherapy) to improve long-term outcomes [3–5]. However, most patients ultimately succumb to relapse due to the incomplete depletion of residual tumor cells [6]. The incorporation of antitumor agents in fibrin sealants has been shown to increase therapeutic efficacy via simultaneous and localized drug delivery during postsurgical wound healing [7–9]. However, the rapid diffusion of small-molecule drugs and disproportionate intracellular delivery of different drugs present formidable challenges for maintaining long-term effects and preventing tumor recurrence.

Embedding nanoparticles within sealants provides a long-acting drug reservoir with extended drug release [10,11]. Moreover, nanomedicines offer significant advantages in the ratiometric codelivery of diverse drugs, enabling synergistic antitumor efficacy [12–14]. Nevertheless, nanomedicines based on chemotherapy only are often insufficient for postsurgical treatment because of the development of an immunosuppressive tumor microenvironment (TME) under surgical stress [15–17]. Thus, triggering robust antitumor immunity during chemotherapy while overcoming adaptive immunosuppression postsurgery is pivotal for complete depletion of residual tumor cells and preventing tumor recurrence [18]. Immunogenic cell death (ICD) inducers, especially when formulated as nanomedicines, are known to elicit antitumor immunity while simultaneously killing tumor cells [19–22]. In addition, strategies that reverse the immunosuppressive TME, such as immune checkpoint blockade and cytokine remodeling, have been clinically utilized and yield certain benefits [23–25].

In this study, we report a chemoimmunotherapeutic fibrin sealant (CI-sealant) to convert the surgical cavity into an in situ "drug-immune depot" with localized release of immunogenic docetaxel/volasertib dual-drug nanocombo (iNCombo) and the transforming growth factor-β

* Corresponding authors at: State Key Laboratory of Bioinspired Interfacial Materials Science, and Biomedical Polymers Laboratory, College of Chemistry, Chemical Engineering and Materials Science, Soochow University, Suzhou 215123, PR China.
*E-mail addresses:* sunhuanli@suda.edu.cn (H. Sun), zyzhong@suda.edu.cn (Z. Zhong).
[1] These authors contributed equally.

https://doi.org/10.1016/j.jconrel.2026.115068
Received 7 February 2026; Received in revised form 31 May 2026; Accepted 3 June 2026
Available online 4 June 2026

(TGF-β) inhibitor galunisertib (Gal) for post-surgery adjuvant therapy (Scheme 1). iNCombo delivers ICD-inducing chemotherapeutic docetaxel (Do) and polo-like kinase 1 (PLK1) inhibitor volasertib (Vo) in a ratiometric manner, evoking synergistic apoptosis and ICD effects in diverse tumor cells. TGF-β is a critical immunosuppressor in the TME that negatively regulates antitumor immunity [26–28]. The incorporation of iNCombo and Gal, as an immunosuppression reliver, into the clinically used fibrin sealant resulted in CI-sealant, which provokes ICD in situ, facilitates T-cell activation and infiltration, and increases the proportion of M1 macrophages, effectively reversing immunosuppression and activating antitumor immunity in a postoperative 4T1-Luc triple-negative breast cancer (TNBC) model. Post-surgery adjuvant therapy with CI-sealant significantly prevents tumor recurrence in both murine 4T1-Luc breast tumor and B16F10 melanoma models, with 71% and 43% of the mice achieving a complete cure, respectively.

## 2. Experimental section

### 2.1. Preparation of iNCombo

iNCombo was obtained from single-step assembly of a poly(ethylene glycol)-*b*-poly(ε-caprolactone-*co*-dithiolane trimethylene carbonate)-mefenamate (PEG-P(CL-DTC)-MA, 2.0-(1.0–1.0) kg/mol, $M_w/M_n$: 1.1, MA grafting ratio: ~100%) copolymer with simultaneous coencapsulation of Do/Vo at mass ratios of 2/1, 1/1, 1/2 and 1/4. In brief, PEG-P(CL-DTC)-MA, Do and Vo were separately dissolved in PEG350 at 300, 100 and 100 mg/mL, respectively, and were then mixed at predetermined ratios. Taking iNCombo with a feeding Do/Vo mass ratio of 1/2 as an example, 0.5 mL of a mixture of polymer (2 mg) and drugs (Do: 0.1 mg, Vo: 0.2 mg) was heated to 60 °C and injected into 9.5 mL of prewarmed phosphate buffer (PB, 10 mM, pH 7.4) at 60 °C, followed by rapid pipetting to form a uniform dispersion. The dispersion was subsequently dialyzed (MWCO: 3.5 kDa) against PB (10 mM, pH 7.4) to obtain iNCombo. Single-drug nanoformulations (iNDo and iNVo) were

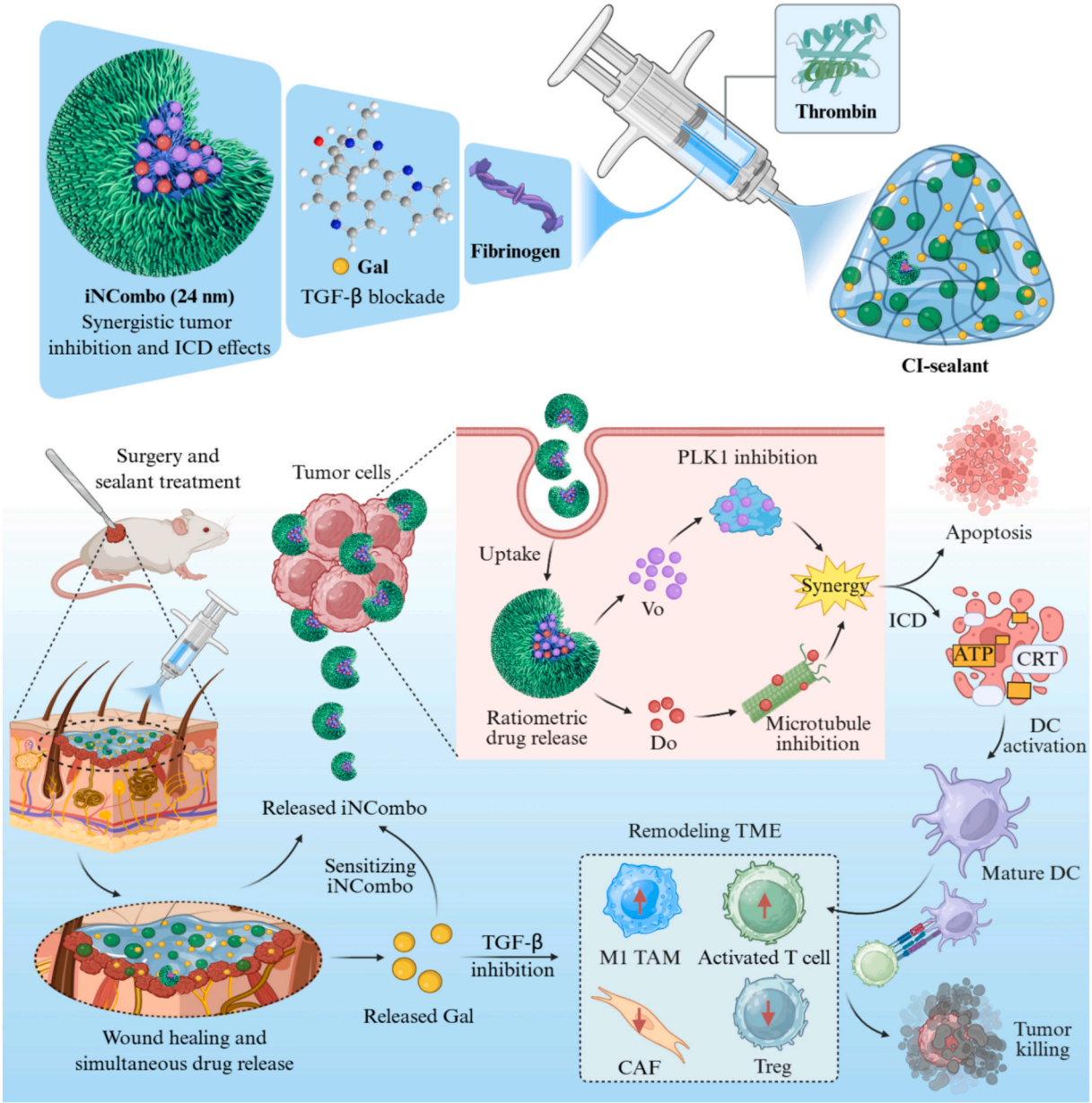


**Scheme 1.** Schematic illustration of the preparation of the immunogenic dual drug iNCombo and TGF-β inhibitor Gal containing chemoimmunotherapeutic fibrin sealant (CI-sealant) for postsurgical adjuvant therapy via synergistic tumor inhibition, ICD stimulation and remodeling of the immunosuppressive TME.

prepared similarly at a theoretical drug loading content (DLC) of 10 wt %. The size and polydispersity index (PDI) of different nanoformulations were measured via DLS. The UV–vis absorption spectra of iNCombo, free Do/Vo (FCombo), iNDo, iNVo and blank nanoformulations (N) were recorded using a UV–vis spectrophotometer. The amount of Do/Vo inside the nanoformulations was quantified via HPLC, and the DLC and drug loading efficiency (DLE) were calculated as follows:

$$\text{DLC}\ (\%) = \frac{\text{Mass of loaded Do or Vo}}{\text{Mass of iNCombo}} \times 100$$

$$\text{DLE}\ (\%) = \frac{\text{Mass of loaded Do or Vo}}{\text{Mass of Do or Vo in feed}} \times 100$$

### 2.2. Stability and in vitro drug release of iNCombo

The changes in the size and PDI of iNCombo against 50-fold dilution with PB, incubation with 10% fetal bovine serum (FBS) or 90 days of storage at 4 °C were monitored via DLS. To determine the drug leakage of iNCombo during storage, 2 mg of iNCombo$_{1/2}$ was sampled, diluted with PB (10 mM, pH 7.4) and ultracentrifuged at 58,000 rpm for 1 h at 4 °C. The amount of free drug in the supernatant was quantified via HPLC. The Do/Vo release from iNCombo was studied in PB (10 mM, pH 7.4) containing 0.5% Tween 80, either with or without 10 mM glutathione (GSH). Then, 0.5 mL of iNCombo$_{1/2}$ (4 mg/mL) was dialyzed (MWCO: 14 kDa) against 20 mL of the corresponding release medium in a thermostatic shaker (37 °C, 100 rpm). At predetermined time points, 5 mL of the release medium was sampled and replaced with an equal volume of fresh medium. The sampled medium was freeze-dried and then redissolved in a mixture of acetonitrile and water (300 μL, 1:1 *v/v*) for HPLC measurements. Each group included three parallel samples.

### 2.3. Cellular uptake and intracellular drug release

The cellular uptake and the intracellular Do/Vo ratio of iNCombo$_{1/2}$ and free Do/Vo$_{1/2}$ (FCombo) were investigated in 4T1-Luc cells. Cells plated in 6-well plates were incubated with iNCombo$_{1/2}$ or FCombo at Do/Vo concentrations of 60/120 μg/mL for 2, 4 or 8 h ($n = 3$). The cells were then collected and lysed with 0.5% Triton X-100. Samples from the FCombo group were directly tested by HPLC, and those from iNCombo$_{1/2}$-treated cells were further incubated with an acetonitrile solution containing DL-dithiothreitol (DTT) to release drugs prior to HPLC measurements. The percentage of Do/Vo delivered into cells and the intracellular Do/Vo ratio were subsequently calculated.

To visualize the cellular uptake and intracellular drug release of iNCombo, Dio- and Dil-coloaded fluorescence resonance energy transfer (FRET) nanoformulations (NDio/Dil) were prepared and incubated with 4T1-Luc cells. In brief, cells were seeded in a 12-well plate containing glass slides ($2 \times 10^5$ cells per well) and incubated with NDio/Dil for 2 h, after which some of the cells were incubated for an additional 2 h with fresh medium. After incubation, the cells were rinsed with PBS, fixed with 1 mL of paraformaldehyde for 15 min, rinsed again, and stained with DAPI (1:1000 dilution in PBS) for 5 min, followed by rinsing with PBS. The cells on the glass slides were mounted onto microscope slides and observed via CLSM at an excitation wavelength of 484 nm.

### 2.4. In vitro synergistic antitumor activity of iNCombo

The synergistic inhibitory effects of iNCombo at different drug ratios on different tumor cell lines, including 4T1-Luc, B16F10, SKOV-3-Luc, ID8 and MC38 cells, were evaluated via the CCK-8 assay. The cells were seeded in 96-well plates at a density of $3 \times 10^3$ cells per well and cultured overnight, followed by 48 h of incubation with iNDo, iNVo, iNCombo$_{2/1}$, iNCombo$_{1/1}$, iNCombo$_{1/2}$ or iNCombo$_{1/4}$ at various concentrations ($n = 6$). Afterward, CCK-8 reagent was added for 4 h incubation, and the absorbance at 450 nm was subsequently recorded with a microplate reader. The cell viability was calculated by comparing the absorbance with that of the PBS group, and the half-maximal inhibitory concentration ($IC_{50}$) was determined by fitting analysis via GraphPad Prism 10 software. The synergistic antitumor effect was evaluated via the combination index (CI) value, which was calculated as follows:

$$\text{CI} = \frac{\text{IC}_{50}\ \text{of Do in iNCombo}}{\text{IC}_{50}\ \text{of iNDo}} + \frac{\text{IC}_{50}\ \text{of Vo in iNCombo}}{\text{IC}_{50}\ \text{of iNVo}}$$

CI $< 1$ indicates synergism, CI $= 1$ indicates an additive effect, and CI $> 1$ indicates antagonism.

The antitumor efficacy of iNCombo$_{1/2}$ in the presence or absence of Gal (50 ng/mL) against 4T1-Luc cells was evaluated similarly at Do concentrations of 0.25, 2.5, 25 and 100 ng/mL. The synergistic effects of free drug combinations (Do/Vo$_{2/1}$, Do/Vo$_{1/1}$, Do/Vo$_{1/2}$ and Do/Vo$_{1/4}$) in 4T1-Luc and B16F10 cells were studied via a similar procedure, with free Do and Vo serving as controls. The cytotoxicity of iNDo, iNVo and iNCombo against mouse BMDCs was assessed similarly by incubating them with BMDCs ($2 \times 10^4$ cells per well) for 24 h.

The proapoptotic ability of iNCombo in 4T1-Luc and B16F10 cells was assessed via an Annexin V-PE/7-AAD double-staining apoptosis kit. The cells were seeded at a density of $2 \times 10^5$ cells per well in a 12-well plate and incubated with PBS, iNDo, iNVo or iNCombo$_{1/2}$ (Do: 60 ng/mL, Vo: 120 ng/mL) for 48 h ($n = 3$). The cells were then digested with trypsin, collected and redispersed into 0.5 mL of binding buffer with subsequent staining with 5 μL of Annexin V-PE and 10 μL of 7-AAD. The stained cells were evaluated by flow cytometry, and the data were processed via FlowJo_V10 software.

### 2.5. iNCombo induces ICD and stimulates BMDC maturation

The ability of iNCombo to induce ICD was assessed in 4T1-Luc and B16F10 cells by measuring cell surface exposure of calreticulin (CRT), together with the concentrations of adenosine triphosphate (ATP) and/or high mobility group box 1 (HMGB1) in the culture medium following different treatments. The cells were incubated with PBS, iNDo, iNVo or iNCombo$_{1/2}$ for 24 h under the same protocol as in the apoptosis experiments. After incubation, the culture medium was subjected to ATP and/or HMGB1 measurement. The cells were digested with trypsin, collected, washed twice with PBS and then blocked with 25 μL of CD16/32 antibody on ice for 15 min. Subsequently, 50 μL of αCRT and 50 μL of Alexa Fluor-labeled secondary antibody were added in sequence and incubated on ice for 1 h and 30 min, respectively. The cells were washed with PBS after each staining step and finally analyzed via flow cytometry.

The maturation of BMDCs stimulated by drug-induced ICD was further explored. The cells were seeded and incubated with PBS, iNDo, iNVo or iNCombo$_{1/2}$ for 24 h as described above. Then, 1 mL of mouse BMDCs ($1 \times 10^6$ cells) was added to each well and further incubated for 24 h. The cells were collected via centrifugation, washed twice with PBS and then blocked with 25 μL of CD16/32 antibody on ice for 15 min. Next, 50 μL of a mixture containing CD11c-FITC, CD80-APC and CD86-PE antibodies was added, and the mixture was incubated on ice in the dark for 30 min. The cells were washed twice with PBS and analyzed via flow cytometry to determine the proportion of $CD11c^+CD80^+CD86^+$ mature BMDCs (mDCs). To study the direct effects of iNCombo on DC maturation, BMDCs were directly incubated with PBS, iNDo, iNVo or iNCombo for 24 h and analyzed as described above.

### 2.6. Preparation of CI-sealant

Fibrinogen and thrombin solutions were separately prepared according to the instruction manual for commercially available porcine fibrin sealant kits to prepare drug-loaded fibrin sealants. Taking the CI-sealant as an example, iNCombo and Gal were mixed with fibrinogen solution first, followed by mixing with thrombin solution at an equal volume, which formed sealants in seconds. I-sealant, $C_{iNDo}$-sealant,

$C_{iNVo}$-sealant, Free C-sealant and C-sealant were fabricated similarly via incorporation of Gal, iNDo, iNVo, FCombo and iNCombo, respectively. The storage modulus and loss modulus of the CI-sealant and the blank fibrin sealant were determined via a rheometer. The morphology of the freeze-dried CI-sealant was characterized by scanning electron microscopy (SEM). Prior to observation, the sample was gold-sputtered for 70 s at 100 mA, and SEM imaging was performed at an accelerating voltage of 15 kV.

To monitor the release of the micelles from the sealants, Cy5-labeled blank nanoformulations (NCy5) were utilized to generate NCy5-sealant, which were immersed in 1 mL of PBS ($n = 3$). A total of 0.5 mL of the release medium was taken out at predetermined time points for fluorescence measurement, and an equal volume of fresh PBS was added. The release of Gal from the I-sealant was evaluated via a similar procedure, and the released Gal was quantified via HPLC. To assess the structural integrity of the micelles released from the sealants, an NDio/Dil FRET nanoformulation-loaded fibrin sealant was prepared for release studies. The released samples collected on days 1.5, 3.5 and 6.5 were measured via a Cary Eclipse fluorescence spectrometer at an excitation wavelength of 484 nm. iNCombo containing C-sealant was further used to study the release of drugs, and the released samples were incubated overnight with acetonitrile containing DTT to destroy the micelles prior to HPLC measurements.

### 2.7. Drug retention at the postsurgical site

All animal procedures were performed in accordance with the Guidelines for Care and Use of Laboratory Animals of Soochow University (China) and approved by the Animal Ethics Committee of Soochow University. To monitor the drug retention at the postsurgical site over time, fibrin sealants incorporating Did-loaded nanoformulations (NDid-sealant) were prepared and applied to a postoperative 4T1-Luc TNBC model for in vivo fluorescence imaging. 4T1-Luc cells suspended in PBS containing 30% Matrigel (50 μL each, $6 \times 10^6$ cells/mL) were inoculated subcutaneously near the right ribs of BALB/c mice. When the tumor volume reached approximately 300 $mm^3$, 95–99% of the tumor was surgically resected with immediate administration of NDid-sealant at the postsurgical site and wound closure (denoted day 0, $n = 3$). The mice were imaged on days 0, 1, 3, 5, and 7 using an in vivo fluorescence imaging system (PerkinElmer IVIS Lumina III). The retention of NDid-sealant was evaluated by measuring the corresponding Did fluorescence intensity at each time point.

### 2.8. Efficacy of CI-sealant in postoperative tumor models

The therapeutic efficacy of CI-sealant was first evaluated in a postoperative 4T1-Luc TNBC model as established above. Bioluminescence imaging was performed one day prior to resection (day −1). Different sealant formulations including I-sealant, $C_{iNDo}$-sealant, $C_{iNVo}$-sealant, Free C-sealant and C-sealant and CI-sealant were applied to the postsurgical site immediately after surgery at Do, Vo and Gal dosages of 8, 16 and 5 mg/kg, respectively. There were 7 mice in each group, and one group of mice that underwent surgery only was used as an untreated control. Bioluminescence imaging was performed to confirm tumor resection and monitor tumor recurrence. Briefly, D-luciferin potassium salt was intraperitoneally administered to mice at a dose of 150 mg/kg 10 min before imaging. The mouse body weights and tumor volumes were continuously tracked. Mouse survival was monitored until spontaneous death or when the tumor volume reached 1500 $mm^3$.

To further validate the therapeutic efficacy of CI-sealant, a postoperative B16F10 model was established in C57BL/6 J mice, which were then treated with C-sealant or CI-sealant via the same procedure as that used for the 4T1-Luc model. One group of untreated mice was used as the control. The body weight, tumor volume and survival of the mice were monitored similarly to those described above.

### 2.9. In vivo immunocyte infiltration analysis

To analyze immunocyte infiltration in vivo, a postoperative 4T1-Luc TNBC model was established and treated with I-sealant, C-sealant or CI-sealant as described above, with one group of untreated controls ($n = 5$). On day 6 post-treatment, all the mice were sacrificed. One mouse from each group was randomly selected, and its major organs and tumors were collected for hematoxylin and eosin (H&E) staining. Moreover, Masson staining and immunofluorescence staining were performed on tumor sections to evaluate fibrosis and the presence of $CD4^+$ T cells, $CD8^+$ T cells, CRT, DCs and macrophages. Peripheral blood, lymph nodes and spleen were isolated from the remaining mice, which were processed into single-cell suspensions and lysed in ACK lysis buffer. Zombie NIR solution (100 μL per sample) was added for 15 min of staining in the dark, followed by washing with PBS. Then, CD16/32 antibody (25 μL per sample) was added, and the mixture was incubated on ice for 15 min. Next, 50 μL of a mixed solution of antibodies specific to T cells (CD45-PerCP/Cy5.5, CD3-APC, CD4-PE, CD8-FITC, CD69-PE/Cy7), Tregs (CD45-PerCP/Cy5.5, CD3-FITC, CD4-PE, CD25-PE/Cy7, FoxP3-APC) and macrophages (CD45-PerCP/Cy5.5, CD11b-FITC, F4/80-PE, CD86-PE/Cy7, CD206-APC) was added, and the mixture was incubated for 30 min on ice. After rinsing with PBS, the samples were analyzed via flow cytometry to detect the infiltration of immune cells.

### 2.10. Statistical analysis

The data are presented as the means ± standard deviations. Statistical analysis was performed via GraphPad Prism 10.0.0 software. One-way ANOVA with Tukey's post hoc test was used for comparisons among different groups. Mouse survival was analyzed via the Kaplan–Meier method and compared via a log-rank (Mantel–Cox) test. $^*p < 0.05$, $^{**}p < 0.01$, $^{***}p < 0.001$, $^{****}p < 0.0001$.

## 3. Results and discussion

### 3.1. Preparation of iNCombo for precise cellular delivery of docetaxel and volasertib

Postsurgical tumors often relapse due to residual tumor cells evading elimination, and the surgical wound fosters an immunosuppressive milieu. Therefore, potent activation of antitumor immunity during adjuvant therapy is pivotal to achieving complete tumor cell depletion and preventing recurrence. Here, we engineered an immunogenic docetaxel/volasertib dual-drug nanocombo (iNCombo) to boost adjuvant chemoimmunotherapy via ratiometric delivery of ICD-inducing chemotherapeutic Do and the PLK1 inhibitor Vo. PLK1 inhibition is recognized for overcoming chemoresistance and synergizing with tubulin-interfering drugs (e.g., Do) [29,30], thereby realizing cooperative tumor inhibition and robust ICD effects. iNCombo, fabricated via single-step self-assembly of the PEG-P(CL-DTC)-MA copolymer, exhibited nearly comparable DLEs for both Do (71.1–88.6%) and Vo (66.9–94.9%), facilitating precise control over Do/Vo ratios (Table S1). Moreover, the encapsulation of Vo together with Do resulted in an obviously greater DLE than that of the Vo-loaded nanoformulations (iNVo, 44.1%). This is presumably attributed to π–π stacking interaction between Do and Vo, which is supported by the obvious red shift of iNCombo in the UV–vis spectra relative to free Do/Vo (FCombo) and single-drug nanoformulations (iNDo and iNVo) (Fig. S1A). iNCombo with controllable Do/Vo mass ratios of 2/1, 1/1, 1/2 and 1/4, denoted as $iNCombo_{2/1}$, $iNCombo_{1/1}$, $iNCombo_{1/2}$ and $iNCombo_{1/4}$, respectively, presented an average size of ca. 24 nm with a low PDI, which were similar to those of iNDo and iNVo (Fig. 1A, S1B). $iNCombo_{1/2}$ with a spherical morphology demonstrated high stability, not only resisting 50-fold dilution or incubation with 10% FBS (Fig. S1C,D) but also maintaining a constant size and size distribution, along with high drug retention during storage at 4 °C for 90 days (Fig. 1B,C). As a result of

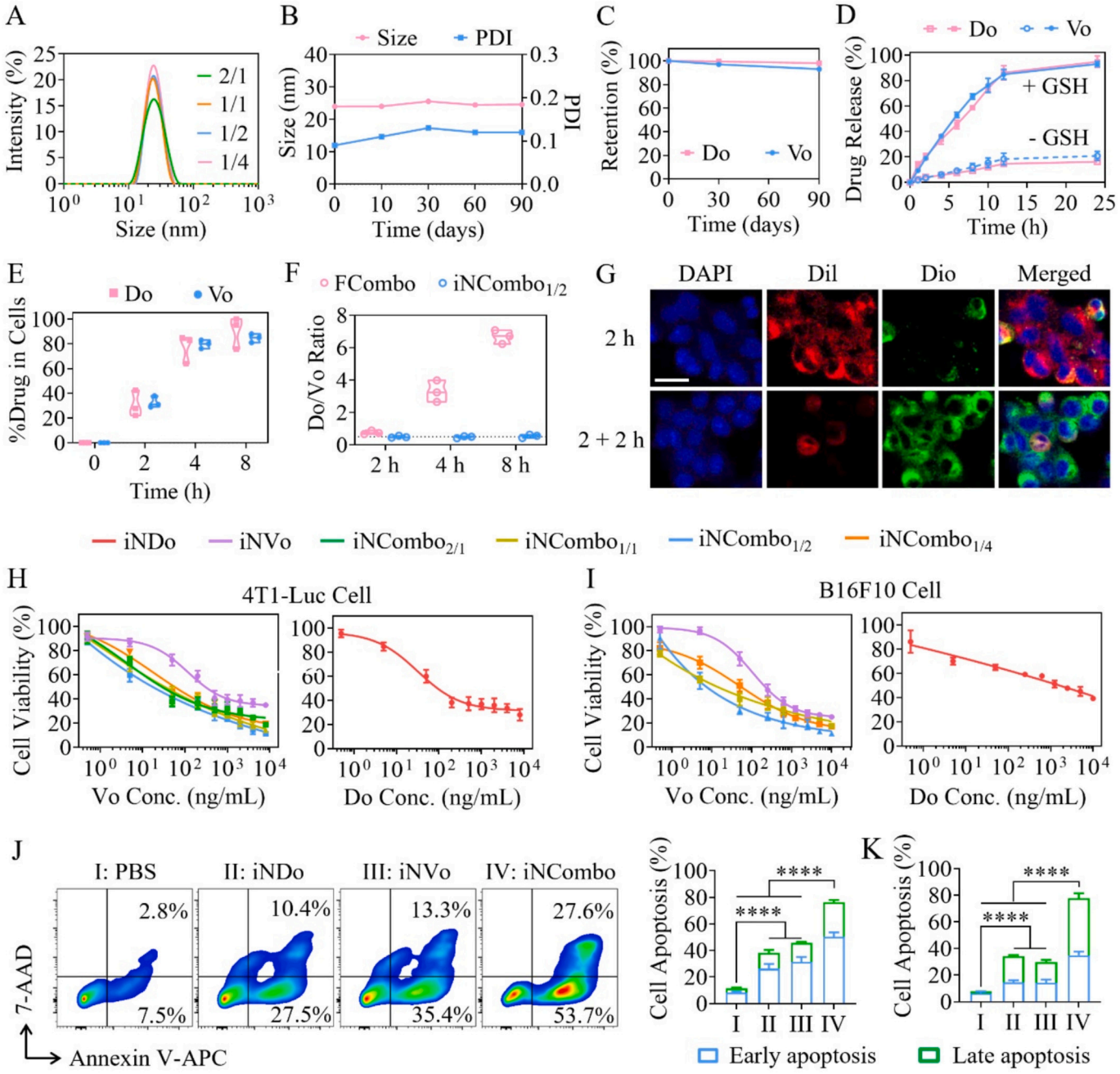


**Fig. 1.** Characterization and in vitro synergistic antitumor activity of iNCombo. (A) Size distributions of iNCombo with various Do/Vo mass ratios. (B) Size and PDI variations and (C) drug retention of $iNCombo_{1/2}$ during storage at 4 °C for 90 days. (D) In vitro Do/Vo release kinetics of $iNCombo_{1/2}$ under different conditions ($n = 3$). (E) Intracellular drug delivery efficiency of $iNCombo_{1/2}$ in 4T1-Luc cells ($n = 3$). (F) Intracellular Do/Vo mass ratios of 4T1-Luc cells after incubation with free Do/$Vo_{1/2}$ combination (FCombo) or $iNCombo_{1/2}$ for different time points ($n = 3$). (G) Cellular uptake and intracellular drug release of FRET nanoformulations (NDio/Dil) in 4T1-Luc cells after 2 h of incubation and a subsequent 2 h incubation in fresh medium (Ex: 484 nm). Scale bars: 25 μm. Antitumor activity of iNCombo, iNDo and iNVo in (H) 4T1-Luc cells and (I) B16F10 cells ($n = 6$). (J) Flow cytometry dot plots and corresponding quantification of apoptosis in 4T1-Luc cells treated with different formulations ($n = 3$). (K) Quantitative analysis of apoptosis of B16F10 cells after different treatments (n = 3). ****$p < 0.0001$.

disulfide crosslinking, $iNCombo_{1/2}$ showed less than 20% Do/Vo leakage after 24 h of incubation at 37 °C and pH 7.4; however, the addition of 10 mM GSH triggered nearly complete release of the two drugs (Fig. 1D). Notably, $iNCombo_{1/2}$ maintained similar release kinetics for Do and Vo in the presence of GSH, which is important for precise intracellular drug corelease and eliciting synergistic effects.

Cellular uptake studies revealed that approximately 80% of Do and Vo were detected within 4T1-Luc cells after 4 h of incubation with $iNCombo_{1/2}$, demonstrating its capacity for rapid and efficient drug codelivery (Fig. 1E). Moreover, the cells incubated with $iNCombo_{1/2}$ for 2–8 h maintained a relatively constant intracellular Do/Vo mass ratio of approximately 1/2, which was in sharp contrast to that of FCombo-treated cells, in which the Do/Vo ratio shifted to 7/1 after 8 h (Fig. 1F). To further visualize the cellular uptake and intracellular release of the dual-drug micelles, classic FRET dye pairs, Dio and Dil, were loaded as model drugs to yield FRET NDio/Dil and incubated with 4T1-Luc cells. As shown in Fig. 1G, NDio/Dil was effectively taken up by the cells at 2 h and showed slight dye release, with strong red fluorescence (Dil) and faint green fluorescence (Dio) in the cytosol. With incubation extended to 4 h, the red fluorescence within the cells markedly

decreased, whereas the green fluorescence notably increased, indicating rapid intracellular drug release.

### 3.2. In vitro synergistic antitumor activity and ICD effects of iNCombo

The synergistic antitumor activity of iNCombo with different drug ratios was evaluated in five solid tumor cell lines (4T1-Luc, B16F10, SKOV3-Luc, ID8 and MC38) via a CCK-8 assay. In 4T1-Luc breast cancer cells, iNCombo with Do/Vo mass ratios of 2/1, 1/1, 1/2 and 1/4 all demonstrated strong synergy in inhibiting cell proliferation, and the strongest synergistic effect was observed for iNCombo$_{1/2,}$ showing a low CI of 0.15 (Fig. 1H and Table S2). Specifically, iNCombo$_{1/2}$ displayed $IC_{50}$ values of 8.6 ng/mL for Do and 17.3 ng/mL for Vo, corresponding to 10.7- and 17.1-fold decreases relative to iNDo (91.7 ng/mL) and iNVo (296.6 ng/mL) single-drug counterparts, respectively. Compared with FCombo, iNCombo$_{1/2}$ demonstrated stronger synergy and 3.5-fold greater antitumor activity (Fig. S2A and Table S3). In B16F10 melanoma cells, iNCombo exhibited much stronger synergistic effects with a CI value as low as 0.03 for iNCombo$_{1/2}$, for which the $IC_{50}$ values were 121.2, 34.3 and 17.1-fold lower than those of iNDo, iNVo and FCombo, respectively (Fig. 1I, S2B and Table S3). In addition to 4T1-Luc and B16F10 cells, iNCombo also exhibited potent synergistic effects on other tumor cells, including MC38 colon cancer, SKOV3-Luc and ID8 ovarian cancer cells, with low CI values of 0.17–0.29 for iNCombo$_{1/2}$ (Fig. S3 and Table S2). In light of the strong synergistic effects of iNCombo$_{1/2}$, it was utilized for further investigation and denoted as iNCombo.

Do and Vo block the mitotic process by inhibiting tubulin depolymerization and PLK1 activity, respectively, thus leading to apoptosis [31–33]. Therefore, the synergistic effect of iNCombo on inducing apoptosis was investigated in 4T1-Luc and B16F10 cells via flow cytometry. iNCombo treatment substantially increased the percentage of apoptotic 4T1-Luc cells from 11.6% (PBS control) to 76.3%, which was significantly higher than that induced by iNDo (38.3%) and iNVo (45.7%) (Fig. 1J). Similarly, iNCombo also induced apoptosis in 78.0% of B16F10 cells, which was 2.2–2.8-fold higher than that in cells treated with single-drug nanoformulations (Fig. 1K, S4).

In addition to provoking apoptosis, Do and Vo have been demonstrated to induce ICD across multiple cancer cells, resulting in the release of damage-associated molecular patterns and subsequent activation of antitumor immunity [34–37]. To validate the synergistic effects of iNCombo on the induction of ICD, we quantified CRT exposure as well as the secretion of ATP and/or HMGB-1 by 4 T1-Luc and B16F10 cells after different treatments. As shown in Fig. 2A, iNDo and iNVo treatment substantially raised the percentage of $CRT^+$ 4T1-Luc cells from 4.8% (in PBS) to 12.1% and 11.5%, respectively. iNCombo treatment further increased CRT exposure with 24.5% of $CRT^+$ cells, which was 5.1-fold greater than that in PBS-treated cells. In addition, iNCombo treatment significantly increased the secretion of ATP and HMGB-1 from 4T1-Luc cells compared to PBS and the iNDo and iNVo single-drug controls (Fig. 2B, S5). Similarly, iNCombo treatment also increased CRT exposure and ATP release in B16F10 cells by 11.8- and 3.2-fold, respectively, which were markedly higher than those of the control formulations (Fig. 2C,D).

The exposure of CRT on the cell surface and the release of ATP are well documented to promote the maturation of dendritic cells (DCs) and thus activate the antitumor immune response [38,39]. Herein, mouse BMDCs were incubated with iNCombo pretreated tumor cells, and their maturation was quantified by determining CD80 and CD86 expression. After incubation with iNCombo-pretreated 4 T1-Luc cells, the proportion of mature BMDCs (mDCs) increased by 11.0% compared with that of PBS-treated cells, which was 2.7- and 4.6-fold higher than the increase in the iNDo and iNVo groups, respectively (Fig. 2E). Similarly, iNCombo-treated B16F10 cells also significantly facilitated the maturation of BMDCs to the greatest extent (Fig. 2F, S6), indicating that the iNCombo-mediated ICD effect could efficiently promote DC maturation. Notably, iNCombo itself was also able to enhance the maturation of BMDCs, similar to iNDo, whereas iNVo had no significant effect (Fig. S7A). It has been reported that Do can induce monocyte differentiation into anti-tumor immune cells, enhance antigen presentation, and is closely associated with innate immune activation [40,41]. Moreover, iNCombo, similar to iNDo and iNVo, exhibited no obvious toxicity to BMDCs even at high Do/Vo concentrations of 200/400 ng/mL (Fig. S7B). Taken together, these results confirmed that iNCombo not only synergistically induced ICD in tumor cells to stimulate DC maturation but also directly activated DCs.

RNA-seq was performed to further elucidate the mechanism underlying the synergistic antitumor effect of iNCombo. Compared with the PBS group, iNCombo treatment induced substantial gene expression changes in 4T1-Luc cells, including 3001 upregulated and 1032 downregulated DEGs (Fig. 2G). Kyoto Encyclopedia of Genes and Genomes (KEGG) analysis showed that the genes regulated by iNCombo were significantly enriched in immune-related pathways, including cytokine–cytokine receptor interaction, as well as the TNF, IL-17, JAK-STAT, Toll-like receptor and PI3K-AKT signaling pathways (Fig. 2H). Moreover, gene heatmaps revealed that iNCombo markedly regulated genes associated with cell cycle arrest and apoptosis (e.g., Cdkn1a, Mapk15, Map3k5, Fas, Casp1), as well as ICD and immune modulation (e.g., Tlr2, Tlr3, Tlr4, Myd88, Cxcl11, JAK3) (Fig. 2I).

### 3.3. Preparation and characterization of chemoimmunotherapeutic fibrin sealant (CI-sealant)

To facilitate the treatment of postoperative tumors, fibrin sealant, which has been clinically approved [42–44], was incorporated with iNCombo and the TGF-β inhibitor Gal. TGF-β inhibition is known to overcome drug resistance on the one hand and reverse the immunosuppressive environment on the other hand [45–47]. A CCK-8 assay revealed that the addition of Gal (50 ng/mL) significantly enhanced the antitumor activity of iNCombo in 4T1-Luc cells at different drug concentrations, whereas Gal itself had no obvious toxicity at concentrations below 1000 ng/mL (Fig. 3A, S8). Moreover, the fibrin sealant was nontoxic to both 4T1-Luc cells and RAW 264.7 cells even at high contents (Fig. S9A). The CI-sealant was facilely prepared by adding iNCombo and Gal into the fibrinogen solution and subsequently mixing it with a thrombin solution (Fig. 3B, S9B). Compared with the blank sealant, the CI-sealant presented a greater storage modulus (G') (Fig. 3C), which was likely attributable to the incorporation of nanoparticles, as observed in previous works [48,49]. Cross-sectional SEM images showed that CI-sealant possessed a porous structure, with iNCombo uniformly dispersed throughout the sealant matrix (Fig. 3D).

To visualize the distribution of iNCombo and monitor its release, Cy5-labeled nanoformulations (NCy5) were utilized to prepare the NCy5-sealant. As shown in the CLSM images, NCy5 was distributed uniformly in the fibrin sealant (Fig. S9C), indicating effective and homogenous encapsulation of the micelles. In addition, encapsulation in the sealant allowed sustained release of NCy5 in 8 days, while Gal was rapidly released in 8 h (Fig. 3E,F). Early-released Gal may preemptively relieve TGF-β-mediated immune suppression and alleviate tumor fibrosis, thereby establishing an immune-permissive state. This could in turn sensitize tumor and immune cells to the immunogenic iNCombo, triggering durable ICD and sustained TME remodeling. To further investigate the integrity and drug retention of iNCombo after release from the sealant, NDio/Dil FRET nanoformulations were encapsulated into the fibrin sealant, and the released NDio/Dil was detected via a fluorescence spectrophotometer at an excitation wavelength of 484 nm. The released NDio/Dil under physiological conditions consistently maintained an intact structure, resulting in limited Dio/Dil leakage within 6.5 days (Fig. 3G). Moreover, treatment of the released samples with DTT led to nearly complete release of both Do and Vo (Fig. 3H). The sustained release of intact iNCombo is beneficial for ratiometric drug delivery to tumor cells, which, in combination with rapid and ratiometric intracellular drug release, is anticipated to maximize synergistic

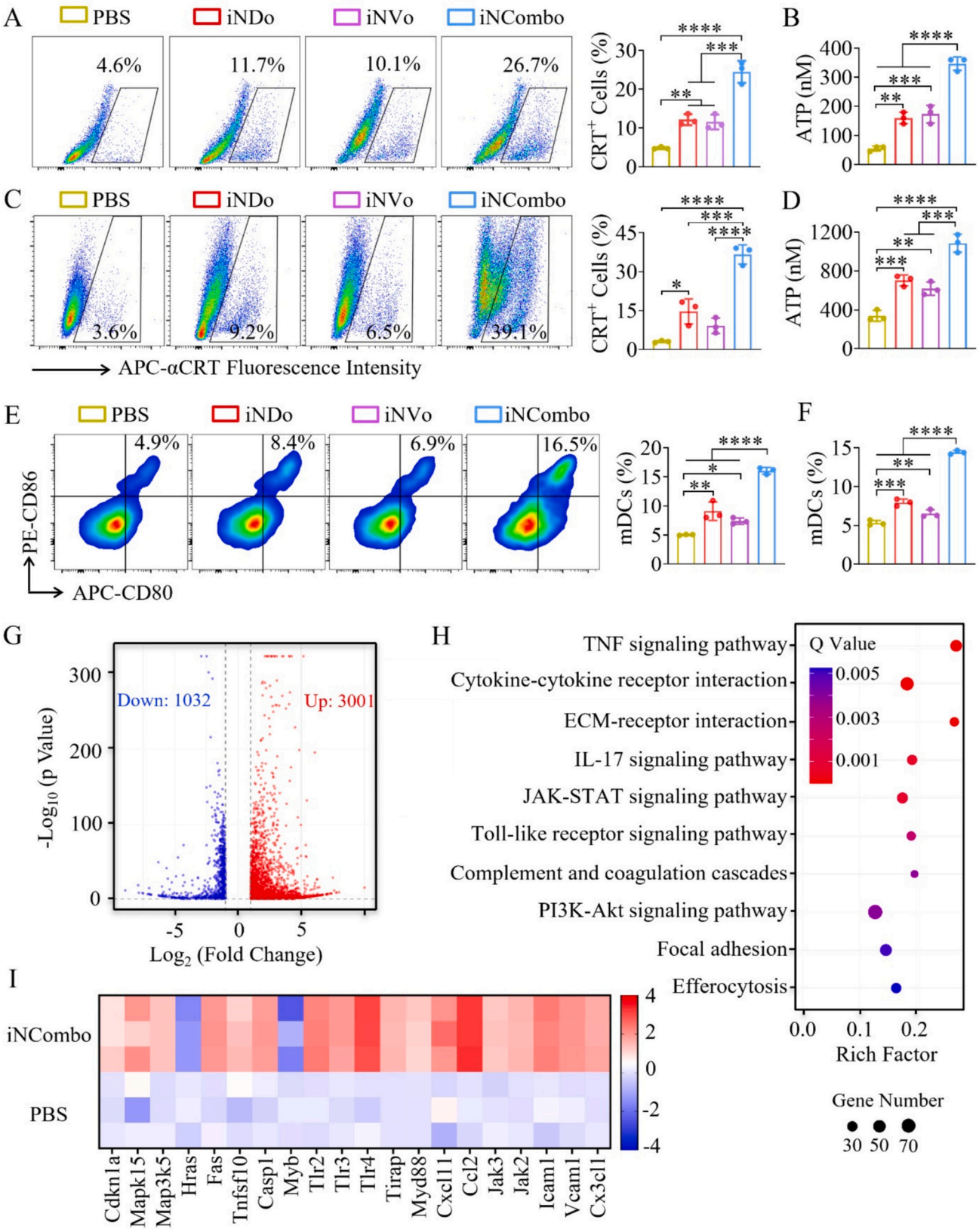


**Fig. 2.** iNCombo stimulates BMDC maturation in vitro and RNA-seq analysis of 4 T1-Luc cells after treatment with iNCombo. (A) CRT exposure and (B) ATP secretion of 4T1-Luc cells following 24 h of incubation with PBS, iNDo, iNVo or iNCombo ($n = 3$). (C) CRT exposure and (D) ATP secretion by B16F10 cells following 24 h of incubation with PBS, iNDo, iNVo or iNCombo ($n = 3$). Matured BMDCs after 24 h of incubation with (E) 4T1-Luc and (F) B16F10 cells pretreated with different formulations ($n = 3$). (G) Volcano plot showing differentially expressed genes (DEGs) between iNCombo and PBS-treated 4T1-Luc cells ($p < 0.05$, $|\text{Log}_2\text{Fold Change}| > 1.0$). (H) KEGG pathway enrichment analysis of 4T1-Luc cells treated with iNCombo versus PBS. (I) Heatmap showing expression of selected genes in iNCombo and PBS treated 4T1-Luc cells ($n = 3$). *$p < 0.05$, **$p < 0.01$, ***$p < 0.001$, ****$p < 0.0001$.

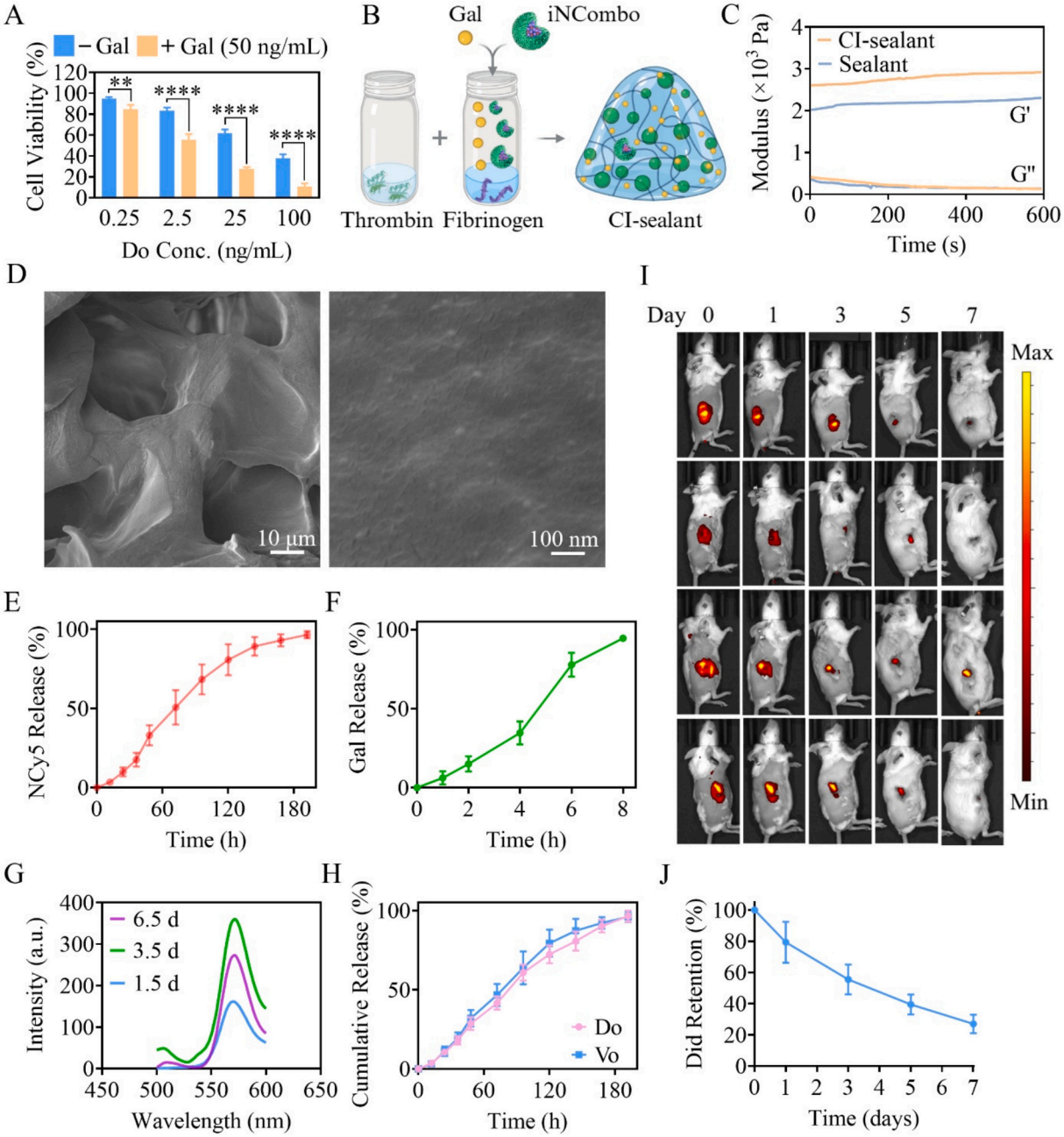


**Fig. 3.** Preparation of CI-sealant for the sustained release of iNCombo and Gal. (A) Viability of 4T1-Luc cells after 48 h of incubation with iNCombo either in the presence or absence of Gal (50 ng/mL, $n = 6$). (B) Schematic of the fabrication of the CI-sealant and (C) its storage and loss modulus. Blank fibrin sealant was used as a control. (D) Cross-sectional SEM images of CI-sealant. Cumulative release of (E) NCy5 and (F) Gal from the fibrin sealant in PBS ($n = 3$). (G) Fluorescence spectra of the release medium of NDio/Dil-sealant at different timepoints. (H) Release profiles of Do and Vo from the CI-sealant after treatment with DTT (n = 3). (I) In vivo fluorescence imaging of postoperative 4T1-Luc mouse model at different timepoints after administration of NDid-sealant at the surgical site and (J) quantitative Did retention analysis ($n = 4$).

antitumor efficacy. The sustained drug release and retention of CI-sealant at the postsurgical site were further studied in a postoperative 4T1-Luc TNBC model using fluorescent NDid-sealant. In vivo fluorescence imaging revealed that the NDid-sealant applied to surgical tumor resection sites effectively retained Did at the surgical area (Fig. 3I). The fluorescence signal gradually decayed over time, with approximately 27% of the signal remaining even 7 days post-administration (Fig. 3J).

### 3.4. CI-sealant for treating the postoperative TNBC model

The therapeutic effects of CI-sealant in inhibiting tumor growth and recurrence after surgery was first evaluated using an incomplete resection 4T1-Luc TNBC model (Fig. 4A). After surgical tumor resection, in situ-formed fibrin sealants containing different formulations, including Gal (I-sealant), iNDo ($C_{iNDo}$-sealant), iNVo ($C_{iNVo}$-sealant), FCombo (Free C-sealant), iNCombo (C-sealant) and CI-sealant, were applied to the surgical cavity at Gal, Do and Vo dosages of 5, 8 and 16 mg/kg, respectively. Surgically resected mice without drug treatment served as controls. Tumor relapse and growth were tracked via both bioluminescence imaging and calipers. As shown in Fig. 4B-E, the mice that were untreated or treated with I-sealant experienced rapid tumor recurrence and growth, with strong bioluminescence signals emerging within one

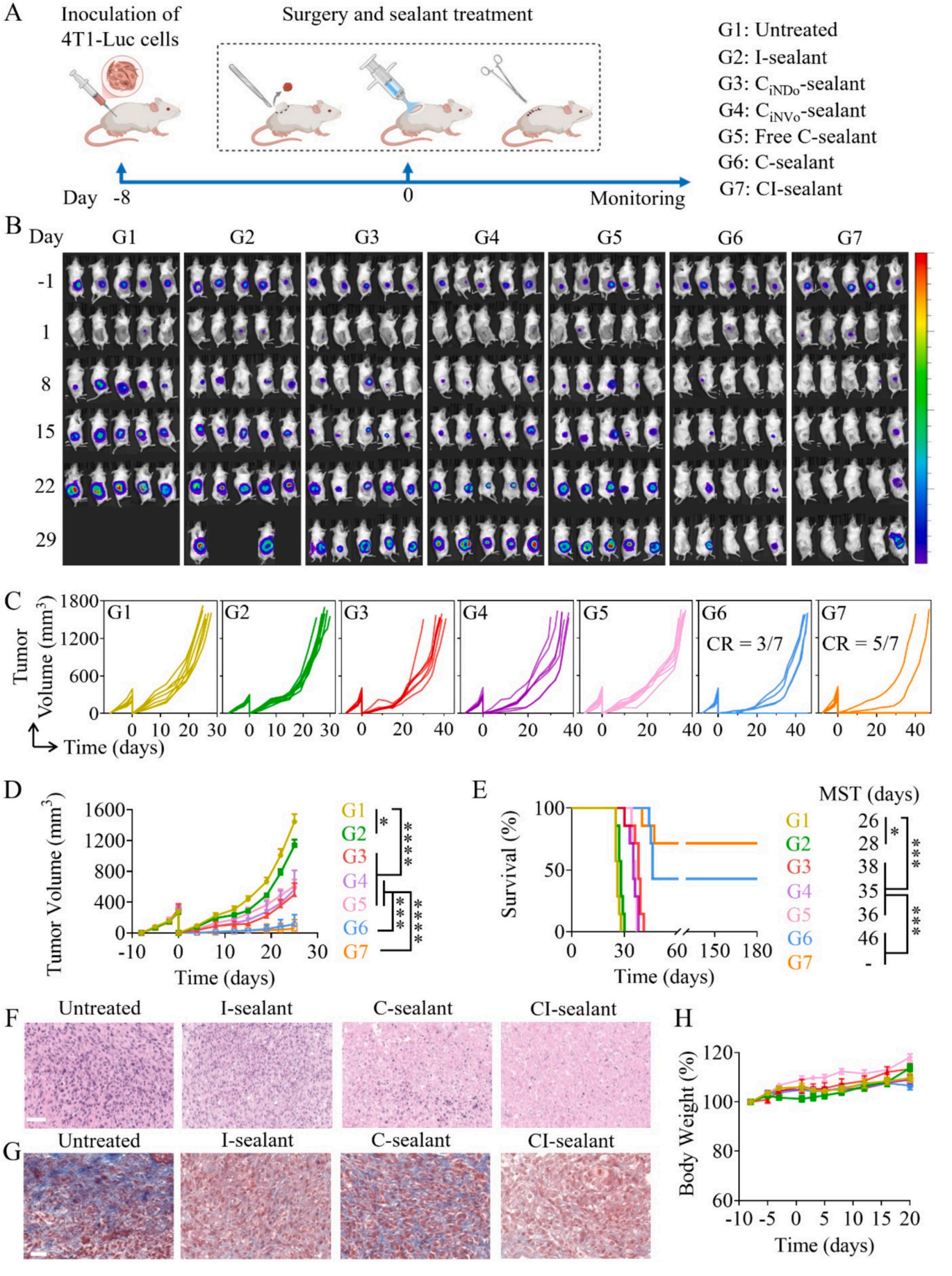


*(caption on next page)*

**Fig. 4.** CI-sealant prevents tumor recurrence in a postoperative 4T1-Luc TNBC model. (A) Schematic illustration of the model establishment and treatment schedule. (B) Representative bioluminescence images of mice treated with different formulations. Untreated mice served as controls. (C) Individual and (D) average tumor growth curves of the mice treated with different sealants ($n = 7$). (E) Survival curves of the mice treated with different sealants ($n = 7$). Representative (F) H&E and (G) Masson-stained images of tumors isolated from untreated mice and those treated with I-sealant, C-sealant, or CI-sealant. Scale bars: 100 μm for F and 25 μm for G. (H) Body weight changes in mice treated with different formulations ($n = 7$). $^{*}p < 0.05$, $^{***}p < 0.001$, $^{****}p < 0.0001$.

week after surgery, and all died within 30 days. The application of $C_{iNDo}$-sealant, $C_{iNVo}$-sealant or Free C-sealant demonstrated certain inhibitory effects and slightly delayed the growth of recurrent tumors, with median survival times extended to 35–38 days, and all the mice died within 41 days. In contrast, treatment with the iNCombo-based C-sealant substantially inhibited tumor recurrence, and 3 out of 7 mice were completely cured with undetectable tumors within 180 days, supporting the synergistic effect of iNCombo. Moreover, CI-sealant incorporating both iNCombo and Gal further significantly enhanced the antitumor efficacy and improved the cure rate, with 5 out of 7 mice achieving complete remission and surviving for at least 180 days.

H&E staining of residual tumors on day 6 post-treatment further confirmed that tumor cell burden in mice treated with C-sealant or CI-sealant was significantly reduced compared to that in the control groups (Fig. 4F). The tumor cells presented evident signs of shrinkage and apoptosis, with the effects being more pronounced in the CI-sealant group. Moreover, the major organs of the mice treated with different formulations all exhibited normal histological morphology (Fig. S10). Masson staining revealed that fibrin sealants incorporating either iNCombo or Gal markedly attenuated tumor-site fibrosis, with CI-sealant resulting in the most significant suppression of fibrotic deposition (Fig. 4G). Reduced fibrosis is recognized for facilitating drug penetration and cytotoxic T lymphocyte infiltration [50,51], which is beneficial for tumor inhibition. Mouse weights increased progressively in all the treatment groups (Fig. 4H). To further evaluate the biosafety of the sealant, wound healing progression was monitored in postsurgical 4T1-Luc TNBC-bearing mice with or without sealant treatment. As shown in Fig. S11A, the wound area in the sealant group decreased gradually over time, showing a healing trend similar to that of the PBS group. Tumor recurrence to some extent hindered complete wound closure in both groups. Moreover, H&E and Masson staining revealed that skin samples from the wound area in the CI-sealant group exhibited a regular histological structure with prominent collagen deposition (Fig. S11B). However, the skin tissue structure in the control group was severely disrupted due to recurrent tumor invasion.

To clarify the immunomodulatory effects, the postoperative 4T1-Luc model was treated with I-sealant, C-sealant, or CI-sealant as described above, with one group of untreated mice serving as controls. Six days after treatment, the tumors, peripheral blood, lymph nodes and spleens were collected for immune cell analysis (Fig. 5A). As shown in Fig. 5B, both the C-sealant and CI-sealant treatments provoked extensive CRT exposure and increased the number of mDCs in the tumor site, indicating that the sustained release of iNCombo effectively triggered ICD and DC maturation in situ. As a consequence, obvious infiltration of $CD4^+$ and $CD8^+$ T cells into the tumor site was also observed in the C-sealant and CI-sealant groups. The latter group demonstrated a more significant effect, which was attributed primarily to the role of Gal in promoting T-cell activation, proliferation and tumor trafficking [52].

Lymph nodes, important sites for the activation of immune cells, play a significant role in tumor immunity [53,54]. Immune cell populations were analyzed by flow cytometry, with the gating strategy shown in Fig. S12. After treatment with either I-sealant or C-sealant, the proportions of $CD3^+CD4^+$ T cells and $CD3^+CD8^+$ T cells significantly increased in the lymph nodes, and the CI-sealant combination further amplified this effect (Fig. 5C,D). Notably, the proportion of activated T cells also markedly increased. Specifically, the number of $CD69^+CD4^+$ T cells in the I-sealant and C-sealant groups was 6.7- and 11.1-fold higher, respectively, than that in the untreated group, and it further increased to 14.3-fold greater in the CI-sealant group (Fig. 5E, S13A). A similar trend was observed for $CD69^+CD8^+$ T cells, with CI-sealant treatment having the best effect; specifically, the number of $CD69^+CD8^+$ T cells increased by 35.1-fold compared with that of the untreated control (Fig. 5F, S13B). Moreover, substantial increases in $CD4^+$ T, $CD8^+$ T and activated T cells were detected in the peripheral blood of the mice treated with different sealant formulations (Fig. 5G-J, and S14). Specifically, the amounts of $CD69^+CD4^+$ T cells and $CD69^+CD8^+$ T cells in the CI-sealant group were 21.5- and 5.9-fold greater than those in the untreated group, respectively (Fig. 5I,J and S15A,B). Furthermore, the percentage of immunosuppressive Tregs in the blood was significantly reduced after different treatments, with the CI-sealant group exhibiting the most pronounced decrease to 5.5%, which was 5.6-fold lower than that of untreated mice (30.8%) (Fig. 5K, S15C).

The spleen serves as a critical hub for immune cells, orchestrating their distribution and function to modulate systemic immune responses. After treatment with CI-sealant, splenomegaly, a typical feature observed in 4T1 tumor-bearing mice [55], was significantly alleviated (Fig. 5L). Additionally, CI-sealant treatment markedly upregulated the levels of $CD4^+$ T, $CD8^+$ T and activated T cells in the spleen and decreased the proportion of Tregs from 9.6% (untreated group) to 0.7% (Fig. 5M-O and S16,17). In addition to modulating T cells, CI-sealant substantially increased the M1 macrophage population in the spleen, increasing their proportion from 21.8% in untreated mice to 63.2%, which was significantly greater than that observed in the I-sealant and C-sealant groups (Fig. 5P, S18A). Nevertheless, the number of M2 macrophages changed negligibly after different treatments, leading to a higher M1/M2 ratio in the combination group (Fig. S18B, C).

### 3.5. CI-sealant for the treatment of postoperative melanoma

To further evaluate the ability of the CI-sealant to prevent tumor recurrence after surgery, a more aggressive postoperative B16F10 melanoma model was established and treated under the same regimen as that used in the postoperative 4T1-Luc model (Fig. 6A). As shown in Fig. 6B-D, the residual tumor recurred rapidly and grew at an accelerated rate, resulting in a short median survival time of only 13 days in the untreated group. C-sealant potently suppressed tumor growth and markedly extended mouse survival, with one mouse surviving for at least 180 days. Notably, CI-sealant treatment further improved potency, with 3 out of 7 mice achieving complete remission and surviving for 180 days. Mouse body weight was stable in all treatment groups over the course of the experiment (Fig. 6E).

## 4. Conclusions

We developed a chemoimmunotherapeutic fibrin sealant (CI-sealant) to convert the surgical cavity into an in situ “drug-immune depot” by sustained release of the immunogenic dual-drug iNCombo and the TGF-β inhibitor Gal, thus preventing postsurgical tumor recurrence. iNCombo, released from CI-sealant, enabled ratiometric codelivery of chemotherapeutic Do and the PLK1 inhibitor Vo, leading to synergistic apoptosis concurrent with ICD effects in different solid tumor cells. The addition of Gal not only increased the antitumor effect of iNCombo but also promoted immune modulation. Post-surgery adjuvant therapy with CI-sealant triggered ICD in situ, stimulated the maturation of BMDCs, promoted the activation of T cells and elicited strong antitumor immunity in vivo, thus effectively inhibiting tumor relapse in postoperative TNBC and melanoma models. This chemoimmunotherapeutic sealant offers a promising postsurgical adjuvant therapy for solid tumors.

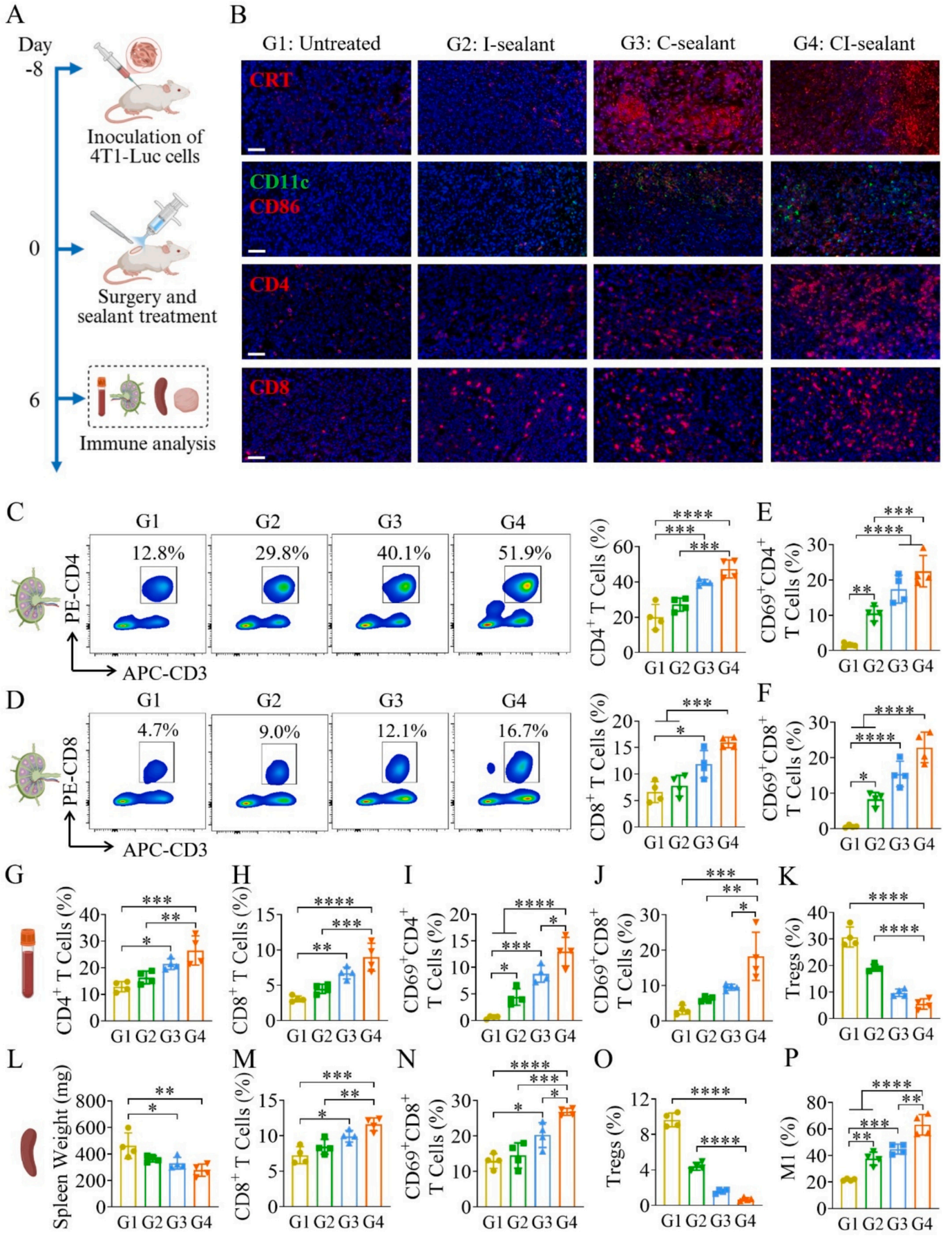


*(caption on next page)*

**Fig. 5.** Immunological analysis of postoperative 4T1-Luc TNBC-bearing mice after different treatments. (A) Treatment schedule. (B) Immunofluorescence images of tumor sections. Scale bars: 50 μm. Representative flow cytometry plots and quantitative analysis of (C) $CD3^+CD4^+$ T and (D) $CD3^+CD8^+$ T cells among $CD45^+$ cells ($n = 4$). Quantitative analysis of (E) $CD69^+CD4^+$ T cells within $CD4^+$ T cells and (F) $CD69^+CD8^+$ T cells within $CD8^+$ T cells in the lymph nodes ($n = 4$). Quantitative analysis of (G) $CD3^+CD4^+$ T cells, (H) $CD3^+CD8^+$ T cells, (I) $CD69^+CD4^+$ T cells, (J) $CD69^+CD8^+$ T cells and (K) Tregs within $CD4^+$ T cells in the peripheral blood ($n = 4$). (L) Spleen weights of the mice in the different treatment groups ($n = 4$). Quantitative analysis of (M) $CD3^+CD8^+$ T cells, (N) $CD69^+CD8^+$ T cells, (O) Tregs among $CD4^+$ T cells and (P) M1 macrophages in the spleen ($n = 4$). $^*p < 0.05$, $^{**}p < 0.01$, $^{***}p < 0.001$, $^{****}p < 0.0001$.

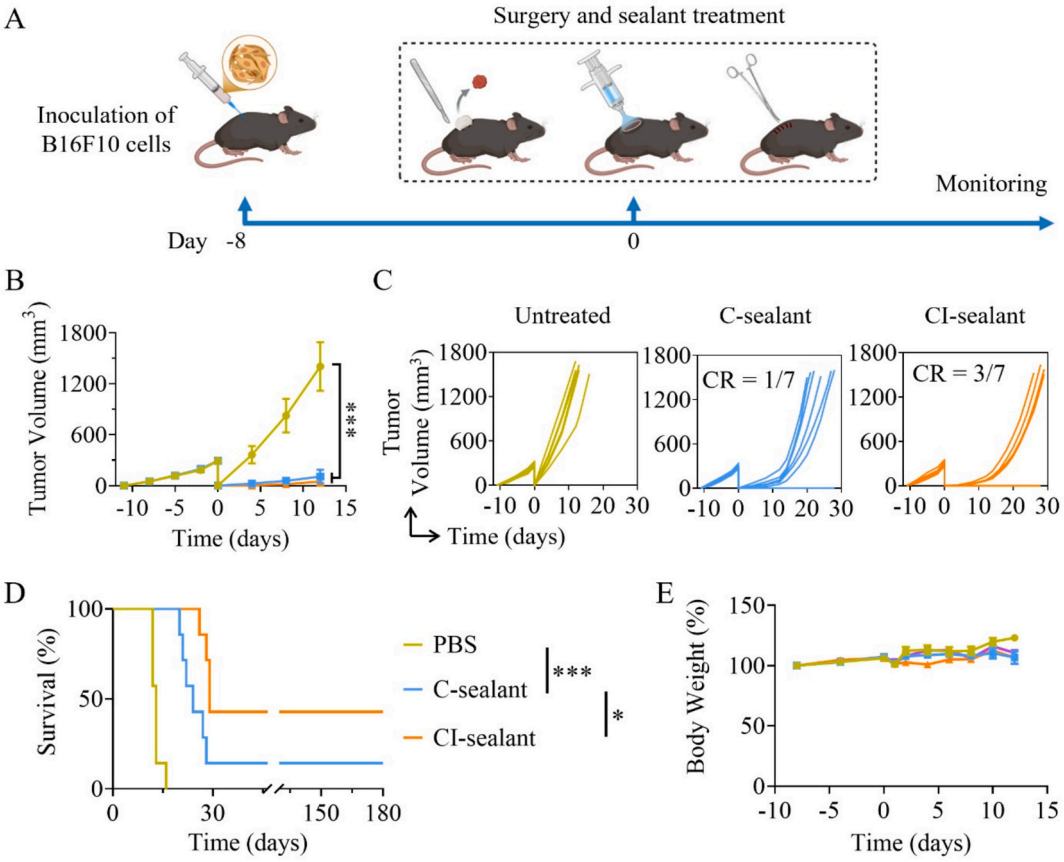


**Fig. 6.** Efficacy of the CI-sealant in treating postoperative B16F10 melanoma-bearing mice. (A) Treatment scheme. (B) Average and (C) individual tumor growth curves of mice treated with different formulations. (D) Survival curves and (E) body weight changes of the mice in the different groups ($n = 7$). $^*p < 0.05$, $^{***}p < 0.001$.

## CRediT authorship contribution statement

**Xueling Tang:** Writing – original draft, Methodology, Investigation, Formal analysis, Data curation. **Jianrong Wang:** Writing – review & editing, Methodology, Investigation, Formal analysis, Data curation. **Lin Chen:** Methodology, Formal analysis. **Yan Zhao:** Methodology, Formal analysis. **Li Cao:** Methodology. **Huanli Sun:** Writing – review & editing, Supervision, Project administration, Funding acquisition, Conceptualization. **Zhiyuan Zhong:** Writing – review & editing, Supervision, Project administration, Funding acquisition, Conceptualization.

## Declaration of competing interest

The authors declare no competing financial interest.

## Acknowledgements

This work was supported by the National Natural Science Foundation of China (52473264, 52273251 and 52233007) and the National Talent Supporting Program of Suzhou (ZXP2025062). The schemes in the figures were created with BioRender.com.

## Appendix A. Supplementary data

Supplementary data to this article can be found online at https://doi.org/10.1016/j.jconrel.2026.115068.

## Data availability

Data will be made available on request.

## References

[1] J.G. Hiller, N.J. Perry, G. Poulogiannis, B. Riedel, E.K. Sloan, Perioperative events influence cancer recurrence risk after surgery, Nat. Rev. Clin. Oncol. 15 (2018) 205–218.
[2] M. Xiao, L. Wang, Q. Tang, Q. Yang, X. Yang, G. Zhu, L. Lei, S. Li, Postoperative tumor treatment strategies: from basic research to clinical therapy, VIEW 5 (2024) 20230117.
[3] S. Li, X. Dan, H. Chen, T. Li, B. Liu, Y. Ju, Y. Li, L. Lei, X. Fan, Developing fibrin-based biomaterials/scaffolds in tissue engineering, Bioact. Mater. 40 (2024) 597–623.
[4] Y. Wang, J. Guo, B. Li, D. Li, Z. Meng, S.-K. Sun, Biocompatible therapeutic albumin/genipin bioglue for postoperative wound adhesion and residual tumor ablation, Biomaterials 279 (2021) 121179.
[5] N.F. Pondé, D. Zardavas, M. Piccart, Progress in adjuvant systemic therapy for breast cancer, Nat. Rev. Clin. Oncol. 16 (2019) 27–44.

[6] Z. Ye, L. Zhou, X. Luo, K. Xue, L. Liang, Z. Meng, P. Zhu, Y. Li, H. Huang, In situ gels for postoperative cancer treatment: current status and challenges, Chem. Eng. J. 505 (2025) 159621.

[7] P. Heher, S. Mühleder, R. Mittermayr, H. Redl, P. Slezak, Fibrin-based delivery strategies for acute and chronic wound healing, Adv. Drug Deliv. Rev. 129 (2018) 134–147.

[8] L. Zhang, J. Zhou, L. Hu, X. Han, X. Zou, Q. Chen, Y. Chen, Z. Liu, C. Wang, In situ formed fibrin scaffold with cyclophosphamide to synergize with immune checkpoint blockade for inhibition of cancer recurrence after surgery, Adv. Funct. Mater. 30 (2020) 1906922.

[9] J. Meng, M. Chen, F. Gu, Y. Miao, Z. Ji, X. Lv, X. Tao, J. Li, Z. Tian, M. Wang, J. Zhang, H. Li, W. You, Z. Wang, Q. Chen, In situ formed chemo-immunotherapeutic hydrogel for suppression of postoperative glioma recurrence and intraoperative hemostasis, J. Control. Release 387 (2025) 114168.

[10] Y. Zhao, L. Cao, S. Zhao, Z. Zhai, X. Tang, L. Chen, H. Sun, Z. Zhong, Polymersomal vincristine-PLK1 inhibitor boosts immunogenic cell death and antitumor immunity, Chem. Eng. J. 518 (2025) 164657.

[11] Y. Lu, H. Ye, J. Zhao, K. Wang, X. Fan, Q. Lu, L. Cao, B. Wan, F. Liu, F. Sun, X. Chen, Z. He, H. Liu, J. Sun, Small EV-based delivery of CpG ODNs for melanoma postsurgical immunotherapy, J. Control. Release 363 (2023) 484–495.

[12] A. Detappe, H.V.T. Nguyen, Y. Jiang, M.P. Agius, W. Wang, C. Mathieu, N.K. Su, S. L. Kristufek, D.J. Lundberg, S. Bhagchandani, I.M. Ghobrial, P.P. Ghoroghchian, J. A. Johnson, Molecular bottlebrush prodrugs as mono- and triplex combination therapies for multiple myeloma, Nat. Nanotechnol. 18 (2023) 184–192.

[13] A.M. Sofias, T. Lammers, Multidrug nanomedicine, Nat. Nanotechnol. 18 (2023) 104–106.

[14] X. Li, X. Peng, M. Zoulikha, G.F. Boafo, K.T. Magar, Y. Ju, W. He, Multifunctional nanoparticle-mediated combining therapy for human diseases, Sig. Transduct. Target. Ther. 9 (2024) 1.

[15] X. Cheng, H. Zhang, A. Hamad, H. Huang, A. Tsung, Surgery-mediated tumor-promoting effects on the immune microenvironment, Semin. Cancer Biol. 86 (2022) 408–419.

[16] F. Tang, Y. Tie, C. Tu, X. Wei, Surgical trauma-induced immunosuppression in cancer: recent advances and the potential therapies, Clin. Transl. Med. 10 (2020) 199–223.

[17] D. Kim, J. Choi, D. Jin, E. Xu, J. Lee, J. Byun, Y.-K. Oh, Hybrid lipid nanoparticles with tumor antigen-primed dendritic cell membranes for post-surgical tumor immunotherapy, J. Control. Release 379 (2025) 537–548.

[18] G. Jin, H. Liu, Z. Mei, Q. Jin, S. Ma, L. Wang, Y. Su, L. Lv, Z. Wang, H. Zhou, M. Li, Z. Huang, X. Chen, S. Lv, Polymeric immunogel prevents tumor recurrence and metastasis by dual activation of innate and adaptive immunity, Bioact. Mater. 45 (2025) 102–114.

[19] L. Galluzzi, E. Guilbaud, D. Schmidt, G. Kroemer, F.M. Marincola, Targeting immunogenic cell stress and death for cancer therapy, Nat. Rev. Drug Discov. 23 (2024) 445–460.

[20] G. Kroemer, C. Galassi, L. Zitvogel, L. Galluzzi, Immunogenic cell stress and death, Nat. Immunol. 23 (2022) 487–500.

[21] Y. Guo, P. Hu, J. Shi, Nanomedicine remodels tumor microenvironment for solid tumor immunotherapy, J. Am. Chem. Soc. 146 (2024) 10217–10233.

[22] K. You, Q. Wang, M.S. Osman, D. Kim, Q. Li, C. Feng, L. Wang, K. Yang, Advanced strategies for combinational immunotherapy of cancer based on polymeric nanomedicines, BMEMat 2 (2024) e12067.

[23] P. Berraondo, M.F. Sanmamed, M.C. Ochoa, I. Etxeberria, M.A. Aznar, J.L. Pérez-Gracia, M.E. Rodríguez-Ruiz, M. Ponz-Sarvise, E. Castañón, I. Melero, Cytokines in clinical cancer immunotherapy, Br. J. Cancer 120 (2019) 6–15.

[24] G. Morad, B.A. Helmink, P. Sharma, J.A. Wargo, Hallmarks of response, resistance, and toxicity to immune checkpoint blockade, Cell 184 (2021) 5309–5337.

[25] M. Wang, F. Yu, Y. Zhang, Present and future of cancer nano-immunotherapy: opportunities, obstacles and challenges, Mol. Cancer 24 (2025) 26.

[26] M. Yi, T. Li, M. Niu, H. Zhang, Y. Wu, K. Wu, Z. Dai, Targeting cytokine and chemokine signaling pathways for cancer therapy, Sig. Transduct. Target. Ther. 9 (2024) 176.

[27] Z. Deng, T. Fan, C. Xiao, H. Tian, Y. Zheng, C. Li, J. He, TGF-β signaling in health, disease and therapeutics, Sig. Transduct. Target. Ther. 9 (2024) 61.

[28] S. Mariathasan, S.J. Turley, D. Nickles, A. Castiglioni, K. Yuen, Y. Wang, E.E. Kadel Iii, H. Koeppen, J.L. Astarita, R. Cubas, S. Jhunjhunwala, R. Banchereau, Y. Yang, Y. Guan, C. Chalouni, J. Ziai, Y. Şenbabaoğlu, S. Santoro, D. Sheinson, J. Hung, J. M. Giltnane, A.A. Pierce, K. Mesh, S. Lianoglou, J. Riegler, R.A.D. Carano, P. Eriksson, M. Höglund, L. Somarriba, D.L. Halligan, M.S. van der Heijden, Y. Loriot, J.E. Rosenberg, L. Fong, I. Mellman, D.S. Chen, M. Green, C. Derleth, G. D. Fine, P.S. Hegde, R. Bourgon, T. Powles, TGFβ attenuates tumour response to PD-L1 blockade by contributing to exclusion of T cells, Nature 554 (2018) 544–548.

[29] Q. Deng, S. Yue, F. You, Z. Zhai, H. Sun, L. Liang, C. Li, L. Yang, Z. Zhong, Vincristine/volasertib polymersome injection enables high-efficiency synergistic treatment of acute lymphoblastic leukemia, Acta Biomater. 200 (2025) 641–652.

[30] S. Su, G. Chhabra, C.K. Singh, M.A. Ndiaye, N. Ahmad, PLK1 inhibition-based combination therapies for cancer management, Transl. Oncol. 16 (2022) 101332.

[31] T. Das, U. Anand, S.K. Pandey, C.R. Ashby, Y.G. Assaraf, Z.-S. Chen, A. Dey, Therapeutic strategies to overcome taxane resistance in cancer, Drug Resist. Updat. 55 (2021) 100754.

[32] J. Van den Bossche, F. Lardon, V. Deschoolmeester, I. De Pauw, J.B. Vermorken, P. Specenier, P. Pauwels, M. Peeters, A. Wouters, Spotlight on volasertib: preclinical and clinical evaluation of a promising plk1 inhibitor, Med. Res. Rev. 36 (2016) 749–786.

[33] S. Yue, Z. Zhai, J. An, H. Sun, J. Li, C. Zhao, Y. Xu, Z. Zhong, Neutrophil/leukemia-tropic dual-drug nanomedicine potentiates the treatment of acute myeloid leukemia, Adv. Mater. 38 (2026) e12635.

[34] Z. Gu, C.G. Da Silva, Y. Hao, T. Schomann, M.G.M. Camps, K. van der Maaden, Q. Liu, F. Ossendorp, L.J. Cruz, Effective combination of liposome-targeted chemotherapy and PD-L1 blockade of murine colon cancer, J. Control. Release 353 (2023) 490–506.

[35] T. Wu, T. Lang, C. Zheng, W. Yan, Y. Li, R. Zhu, X. Huang, H. Xu, Y. Li, Q. Yin, Promote intratumoral drug release and penetration to counteract docetaxel-induced metastasis by photosensitizer-modified red blood cell membrane-coated nanoparticle, Adv. Funct. Mater. 33 (2023) 2212109.

[36] J. Li, Y. Dai, T. Wang, X. Zhang, P. Du, Y. Dong, Z. Jiao, Polyphenol-based pH-responsive nanoparticles enhance chemo-immunotherapy in pancreatic cancer, J. Control. Release 380 (2025) 615–629.

[37] L. Liang, Z. Zhai, W. Lin, L. Cao, H. Sun, Z. Zhong, In situ generation of anti-leukemia vaccine by immunogenic dual-drug nanomedicine and polymersomal CpG nanoadjuvant, J. Colloid Interface Sci. 699 (2025) 138144.

[38] D. Ding, X. Jiang, Advances in immunogenic cell death for cancer immunotherapy, Small Methods 7 (2023) 2300354.

[39] Y. Engelen, R. Demuynck, J. Ramon, K. Breckpot, S.C. De Smedt, G.P.R. Lajoinie, K. Braeckmans, D.V. Krysko, I. Lentacker, Immunogenic cell death as interplay between physical anticancer modalities and immunotherapy, J. Control. Release 384 (2025) 113721.

[40] C.R. Millrud, M. Mehmeti, K. Leandersson, Docetaxel promotes the generation of anti-tumorigenic human macrophages, Exp. Cell Res. 362 (2018) 525–531.

[41] Y. Tezuka, K. Kawasaki, Y. Sumitomo, M. Saito, A. Yao, M. Ando, Docetaxel-induced immune activation shows antitumor synergy with the tumor-targeted CD40 agonist KK2269, Cancer Sci. (2026), https://doi.org/10.1111/cas.70376.

[42] R. Reichsöllner, P. Heher, J. Hartmann, S. Manhartseder, R. Singh, H. Gulle, P. Slezak, A comparative high-resolution physicochemical analysis of commercially available fibrin sealants: impact of sealant osmolality on biological performance, J. Biomed. Mater. Res., Part A 111 (2023) 488–501.

[43] Q. Chen, C. Wang, X. Zhang, G. Chen, Q. Hu, H. Li, J. Wang, D. Wen, Y. Zhang, Y. Lu, G. Yang, C. Jiang, J. Wang, G. Dotti, Z. Gu, In situ sprayed bioresponsive immunotherapeutic gel for post-surgical cancer treatment, Nat. Nanotechnol. 14 (2019) 89–97.

[44] H. Montazerian, E. Davoodi, A. Baidya, S. Baghdasarian, E. Sarikhani, C.E. Meyer, R. Haghniaz, M. Badv, N. Annabi, A. Khademhosseini, P.S. Weiss, Engineered hemostatic biomaterials for sealing wounds, Chem. Rev. 122 (2022) 12864–12903.

[45] B.-G. Kim, E. Malek, S.H. Choi, J.J. Ignatz-Hoover, J.J. Driscoll, Novel therapies emerging in oncology to target the TGF-β pathway, J. Hematol. Oncol. 14 (2021) 55.

[46] X. Wang, P.J.A. Eichhorn, J.P. Thiery, TGF-β, EMT, and resistance to anti-cancer treatment, Semin. Cancer Biol. 97 (2023) 1–11.

[47] X. Shi, J. Yang, S. Deng, H. Xu, D. Wu, Q. Zeng, S. Wang, T. Hu, F. Wu, H. Zhou, TGF-β signaling in the tumor metabolic microenvironment and targeted therapies, J. Hematol. Oncol. 15 (2022) 135.

[48] X. Xue, H. Zhang, H. Liu, S. Wang, J. Li, Q. Zhou, X. Chen, X. Ren, Y. Jing, Y. Deng, Z. Geng, X. Wang, J. Su, Rational design of multifunctional CuS nanoparticle-PEG composite soft hydrogel-coated 3D hard polycaprolactone scaffolds for efficient bone regeneration, Adv. Funct. Mater. 32 (2022) 2202470.

[49] L. Mao, L. Wang, M. Zhang, M.W. Ullah, L. Liu, W. Zhao, Y. Li, A.A.Q. Ahmed, H. Cheng, Z. Shi, G. Yang, In situ synthesized selenium nanoparticles-decorated bacterial cellulose/gelatin hydrogel with enhanced antibacterial, antioxidant, and anti-inflammatory capabilities for facilitating skin wound healing, Adv. Healthc. Mater. 10 (2021) 2100402.

[50] P. Hua, D. Jiang, Z. Guo, H. Tian, X. Chen, M. Chen, Amplified cancer immunotherapy of PD-L1 blockade by sequential tumor microenvironment reshaping and DC maturation, Chem. Eng. J. 453 (2023) 139795.

[51] M. Zhou, J. Wang, J. Pan, H. Wang, L. Huang, B. Hou, Y. Lai, F. Wang, Q. Guan, F. Wang, Z. Xu, H. Yu, Nanovesicles loaded with a TGF-β receptor 1 inhibitor overcome immune resistance to potentiate cancer immunotherapy, Nat. Commun. 14 (2023) 3593.

[52] A.J. Gunderson, T. Yamazaki, K. McCarty, N. Fox, M. Phillips, A. Alice, T. Blair, M. Whiteford, D. O'Brien, R. Ahmad, M.X. Kiely, A. Hayman, T. Crocenzi, M. J. Gough, M.R. Crittenden, K.H. Young, TGFβ suppresses CD8+ T cell expression of CXCR3 and tumor trafficking, Nat. Commun. 11 (2020) 1749.

[53] C.J.H. Porter, N.L. Trevaskis, Targeting immune cells within lymph nodes, Nat. Nanotechnol. 15 (2020) 423–425.

[54] I. Delclaux, K.S. Ventre, D. Jones, A.W. Lund, The tumor-draining lymph node as a reservoir for systemic immune surveillance, trends, Cancer 10 (2024) 28–37.

[55] Z. Luo, Y. Lu, Y. Shi, M. Jiang, X. Shan, X. Li, J. Zhang, B. Qin, X. Liu, X. Guo, J. Huang, Y. Liu, S. Wang, Q. Li, L. Luo, J. You, Neutrophil hitchhiking for drug delivery to the bone marrow, Nat. Nanotechnol. 18 (2023) 647–656.